Nanoscale Research Letters
a SpringerOpen Journal

NANO EXPRESS Open Access

Lead-free $LiNbO_3$ nanowire-based nanocomposite for piezoelectric power generation

Byung Kil Yun[1], Yong Keun Park[1], Minbaek Lee[1], Nuri Lee[2], William Jo[2], Seongsu Lee[3] and Jong Hoon Jung[1*]

Abstract

In a flexible nanocomposite-based nanogenerator, in which piezoelectric nanostructures are mixed with polymers, important parameters to increase the output power include using long nanowires with high piezoelectricity and decreasing the dielectric constant of the nanocomposite. Here, we report on piezoelectric power generation from a lead-free $LiNbO_3$ nanowire-based nanocomposite. Through ion exchange of ultra-long $Na_2Nb_2O_6$-H_2O nanowires, we synthesized long (approximately 50 μm in length) single-crystalline $LiNbO_3$ nanowires having a high piezoelectric coefficient (d_{33} approximately 25 pmV^{-1}). By blending $LiNbO_3$ nanowires with poly(dimethylsiloxane) (PDMS) polymer (volume ratio 1:100), we fabricated a flexible nanocomposite nanogenerator having a low dielectric constant (approximately 2.7). The nanogenerator generated stable electric power, even under excessive strain conditions (approximately 10^5 cycles). The different piezoelectric coefficients of d_{33} and d_{31} for $LiNbO_3$ may have resulted in generated voltage and current for the e_{33} geometry that were 20 and 100 times larger than those for the e_{31} geometry, respectively. This study suggests the importance of the blending ratio and strain geometry for higher output-power generation in a piezoelectric nanocomposite-based nanogenerator.

Keywords: High and stable electric power; Lead-free $LiNbO_3$ nanowire; Nanocomposite nanogenerator
PACS: 77.65.-j; 77.84.-s; 73.21.Hb

Background

Lead-based piezoelectric materials, such as $Pb(Zr,Ti)O_3$ and $Pb(Mg,Nb)O_3$-$PbTiO_3$, have been utilized for the last several decades in actuators, transducers, and sensor applications [1]. As the restriction of hazardous substances becomes an emerging issue, however, much attention has been paid to lead-free piezoelectric materials having a perovskite structure [2]. Among the candidates to replace toxic lead-based piezoelectric materials, alkaline niobates, such as $(K,Na,Li)NbO_3$, are regarded as one of the most appropriate materials due to their high Curie temperature, piezoelectric coefficient, and electromechanical coupling coefficient [3,4].

In addition to nanoelectromechanical system (NEMS) applications, one of the most challenging applications of nanosize lead-free piezoelectric materials is the nanogenerator, which can effectively convert ubiquitous mechanical vibrations into electricity [5]. Due to the low power consumption of modern devices, lead-free piezoelectric nanostructure-based nanogenerators could be a powerful alternative to batteries. Until recently, several nanogenerators have been reported using $BaTiO_3$, $ZnSnO_3$, $Pb(Zr,Ti)O_3$, $Pb(Mg,Nb)O_3$-$PbTiO_3$, and $(K,Na)NbO_3$ [6-11]. In particular, piezoelectric nanocomposite devices, in which piezoelectric nanostructures are mixed with flexible polymers, have exhibited relatively easy, cost-effective fabrication, and high-power generation [9-13]. In a flexible nanocomposite-based nanogenerator, important parameters to increase the output power include using long nanowires with high piezoelectricity and decreasing the dielectric constant of the nanocomposite [9].

In this paper, we report on piezoelectric power generation from a lead-free $LiNbO_3$ nanowire-based composite device. As for the nanogenerator applications, $LiNbO_3$ has several merits such as small dielectric constant, relatively high piezoelectric constant, and thermal stability [14,15]. Through successful ion exchange in microporous $Na_2Nb_2O_6$-H_2O nanowires, we synthesized long (approximately 50 μm) $LiNbO_3$ nanowires having high piezoelectricity (approximately 25 pmV^{-1}). By mixing

* Correspondence: jhjung@inha.ac.kr
[1]Department of Physics, Inha University, Incheon 402-751, Republic of South Korea
Full list of author information is available at the end of the article

$LiNbO_3$ and poly(dimethylsiloxane) (PDMS) (in a volume ratio of 1:100, respectively), we fabricated a flexible nanogenerator having a low dielectric constant for the e_{33} and e_{31} geometries. For a similar value of strain, we note that the open-circuit voltage and closed-circuit current for the e_{33} geometry were 20 and 100 times larger than those for the e_{31} geometry, respectively. For up to 10^5 cycles of strain, we observed that the generated power was quite stable; the dielectric constant and electric loss did not change significantly.

Methods

High-quality $LiNbO_3$ nanowires were synthesized using a three-step procedure. First, we obtained microporous $Na_2Nb_2O_6$-H_2O nanowires by a hydrothermal method. NaOH (12 M) was dissolved in 20 mL of distilled water; 0.113 M of Nb_2O_5 was then added to the NaOH solution. The solution was stirred and transferred into a 25-mL Teflon lining in a stainless steel autoclave to undergo a hydrothermal reaction at 120°C for 5 h. In the second step, we obtained $Li_2Nb_2O_6$-H_2O nanowires using the ion-exchange method. LiCl (20 M) was dissolved in 20 mL of distilled water. $Na_2Nb_2O_6$-H_2O nanowires were added to the LiCl solution. After stirring for 20 h, the stirred solution was filtered, washed with distilled water, and dried at 80°C for 12 h. In the third step, $LiNbO_3$ nanowires were obtained after heating the ion-exchanged $Li_2Nb_2O_6$-H_2O nanowires at 500°C for 2 h.

The crystalline structure of the nanowires was characterized by high-resolution X-ray diffraction (HR-XRD), field-emission scanning electron microscopy (FE-SEM), and field-emission transmission electron microscopy (FE-TEM) measurements. To characterize the detailed crystal structure and symmetry, we performed neutron diffraction measurements and a Rietveld analysis. We used piezoresponse force microscopy (PFM) to investigate the piezoelectricity and piezoelectric/ferroelectric domains of the $LiNbO_3$ nanowires. The PFM measurements were performed using an atomic force microscope at 1 V and 73 kHz. To scan the surface, we used Pt/Ir-coated tips and a force constant of 3 Nm^{-1}. Before scanning, we thoroughly dispersed and tightly attached the nanowires to the Pt-coated Si substrate using a polymer (5 wt.% poly(vinylpyrrolidone) dissolved in ethanol). The $LiNbO_3$ nanowires were then coated with 10-nm-thick Pt to obtain a uniform electric field and to minimize electrostatic effects.

To fabricate the nanocomposite nanogenerator, the $LiNbO_3$ nanowires were thoroughly mixed with PDMS at a volume ratio of 1:100. (We noted that $LiNbO_3$ nanowires were not mixed well with PDMS for an increased volume ratio of 2:100.) Small amounts of the mixture were spin-coated onto an Au/Cr-coated Kapton polyimide film at 500 rpm for 10 s. The 25-nm-thick Au and 10-nm-thick Cr films were deposited onto the Kapton film by thermal evaporation. Another Au/Cr-coated Kapton film was attached to the top surface of the spin-coated $LiNbO_3$-PDMS composite for the electrode. Finally, polyester (PS) film was attached to the bottom Kapton film. The thicknesses of the Kapton and PS films were 125 and 500 μm, respectively. We applied an electric field of approximately 100 $kV \cdot cm^{-1}$ for electric poling at room temperature [16].

To measure the Young's modulus of the $LiNbO_3$-PDMS composite, we used a nanoindenter with a Berkovich tip, and applied the continuous stiffness measurement option. A linear motor was used to periodically apply and release compressive force at a frequency of 0.8 Hz. The pushing and bending amplitudes were varied over the course of the measurement. The output signal of the piezoelectric device was recorded by low-noise voltage and current preamplifiers.

Results and discussion

Microporous $Na_2Nb_2O_6$-H_2O nanowires seem to be an excellent template for ion exchange [17]. Due to the smaller ionic size of the lithium ion (Li^+) compared with the sodium ion (Na^+), as well as the excessive amount of LiCl (i.e., approximately 20 M), all of the Na^+ appeared to be involved in the exchange with Li^+ in $Na_2Nb_2O_6$-H_2O. Figure 1a compares the XRD pattern of $Li_2Nb_2O_6$-H_2O and $Na_2Nb_2O_6$-H_2O. The overall XRD pattern of $Li_2Nb_2O_6$-H_2O was quite different from that of $Na_2Nb_2O_6$-H_2O. From an inductive-coupled plasma (ICP) measurement of $Li_2Nb_2O_6$-H_2O, we did not find any trace of Na^+ within the experimental limits. These results imply that crystalline $Li_2Nb_2O_6$-H_2O could be obtained from $Na_2Nb_2O_6$-H_2O through an ion exchange process.

In Figure 1b, we show *in-situ* XRD patterns of $Li_2Nb_2O_6$-H_2O at elevated temperatures. The diffraction patterns of $Li_2Nb_2O_6$-H_2O were significantly modified with an increase in temperature, especially above 400°C, and exhibited an irreversible phase transformation. In the inset of Figure 1a, we show the XRD pattern after heat treatment of $Li_2Nb_2O_6$-H_2O. We note that the XRD pattern obtained after heat treatment was well indexed by $LiNbO_3$. To the best of our knowledge, this is the first report for the synthesis of $LiNbO_3$ nanowire through ion exchange and subsequent heat treatment.

To gain insight into the phase transformation from $Li_2Nb_2O_6$-H_2O to $LiNbO_3$, we show the thermogravimetric (TG) and differential scanning calorimetry (DSC) results in Figure 1c. The mass of $Li_2Nb_2O_6$-H_2O changed significantly near 400°C and was accompanied by endothermic reactions at the same temperature. After the endothermic reactions, an exothermic reaction occurred near 460°C without a noticeable change in the mass. Comparing the well-known phase transformation mechanism from

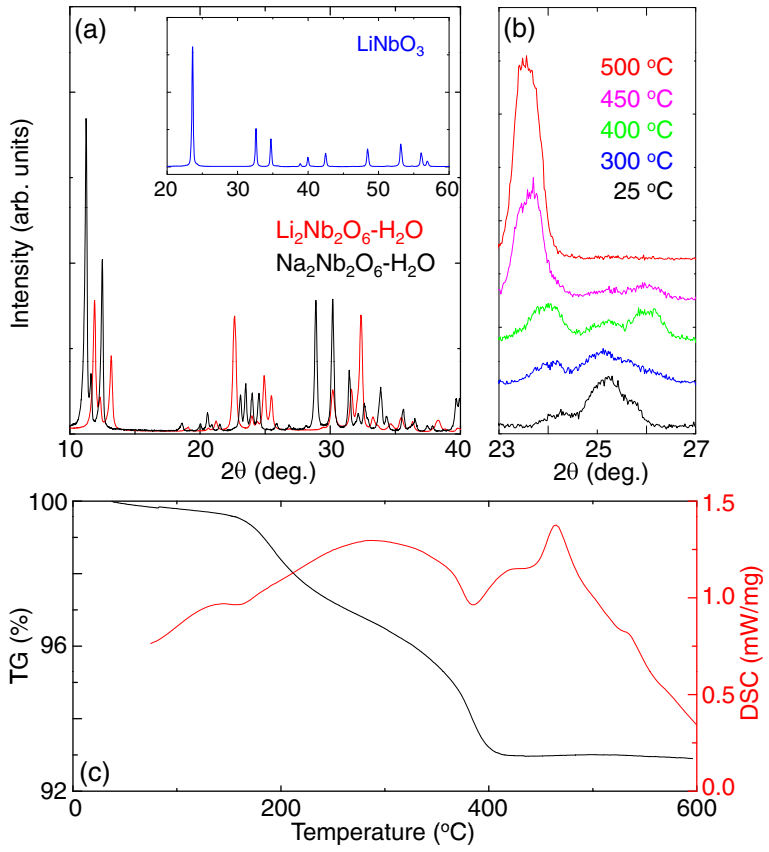

Figure 1 Phase transformation from $Li_2Nb_2O_6$-H_2O to $LiNbO_3$. High-resolution X-ray diffraction (HR-XRD) patterns of $Li_2Nb_2O_6$-H_2O at **(a)** room temperature and **(b)** elevated temperatures. In (a), we show the XRD patterns of $Na_2Nb_2O_6$-H_2O and $LiNbO_3$ for comparison. **(c)** Thermogravimetric (TG) and differential scanning calorimetry (DSC) results for $Li_2Nb_2O_6$-H_2O.

$Na_2Nb_2O_6$-H_2O to $NaNbO_3$ [18], the peaks at 400°C and 460°C corresponded well to the dehydration of H_2O from $Li_2Nb_2O_6$-H_2O and the structural transformation from $Li_2Nb_2O_6$ to $LiNbO_3$, respectively. (The broad change in the mass near 220°C seems to have originated from the desorption of surface/lattice-absorbed hydroxyl defects [19]).

Due to the light Li ions, we used neutrons rather than X-rays to determine the detailed crystal structure of $LiNbO_3$. Figure 2a shows a Rietveld analysis of the neutron diffraction pattern of $LiNbO_3$. The neutron diffraction pattern of $LiNbO_3$ was well-fit by the trigonal structure (a = 5.488 Å, α = 55.89°) with *R3c* symmetry. The resulting lattice constant (angle) of the $LiNbO_3$ nanostructure was slightly smaller (larger) than that of the $LiNbO_3$ single crystal (a = 5.492 Å, α = 55.53°) [20]. Based on the Rietveld analysis, we show the crystal structure of $LiNbO_3$ in the inset of Figure 2a. The Nb ions in the NbO_6 octahedra shifted toward the [111] direction, hence initiating the spontaneous formation of electric polarization without applying an electric field.

Figure 2b,c shows FE-SEM and HR-TEM images of $LiNbO_3$, respectively. All of the $LiNbO_3$ samples had nanowire morphology, with a high aspect ratio of 160 to 600 (width 100 to 250 nm; length 40 to 60 μm). Note that the $LiNbO_3$ nanowires, synthesized using the molten salt method, had a relatively short length (<10 μm) [21]. The clear lattice fringe indicated the single-crystalline quality of the $LiNbO_3$ nanowires. Based on the Rietveld analysis, the $LiNbO_3$ nanowires appeared to grow along the [1-10] direction.

To investigate the piezoelectricity of the $LiNbO_3$ nanowires, we used PFM. Figure 3a,b,c shows the topography, amplitude, and phase of the piezoelectric response of a single $LiNbO_3$ nanowire, respectively. The brightness of the amplitude map represents the strength of the piezoelectric response; the contrast of the phase map corresponds to the direction of the electric polarization in the nanowire. From Figure 3b, c, the piezoelectric domains in the $LiNbO_3$ nanowire were clearly evident.

Figure 3d,e shows the switching of the piezoelectric/ferroelectric amplitude and phase with the application of direct-current (dc) voltage. An abrupt change in the phase suggests the switching of domains in $LiNbO_3$, which is generally associated with ferroelectric behavior [22]. We estimated the piezoelectric coefficient d_{33} value from

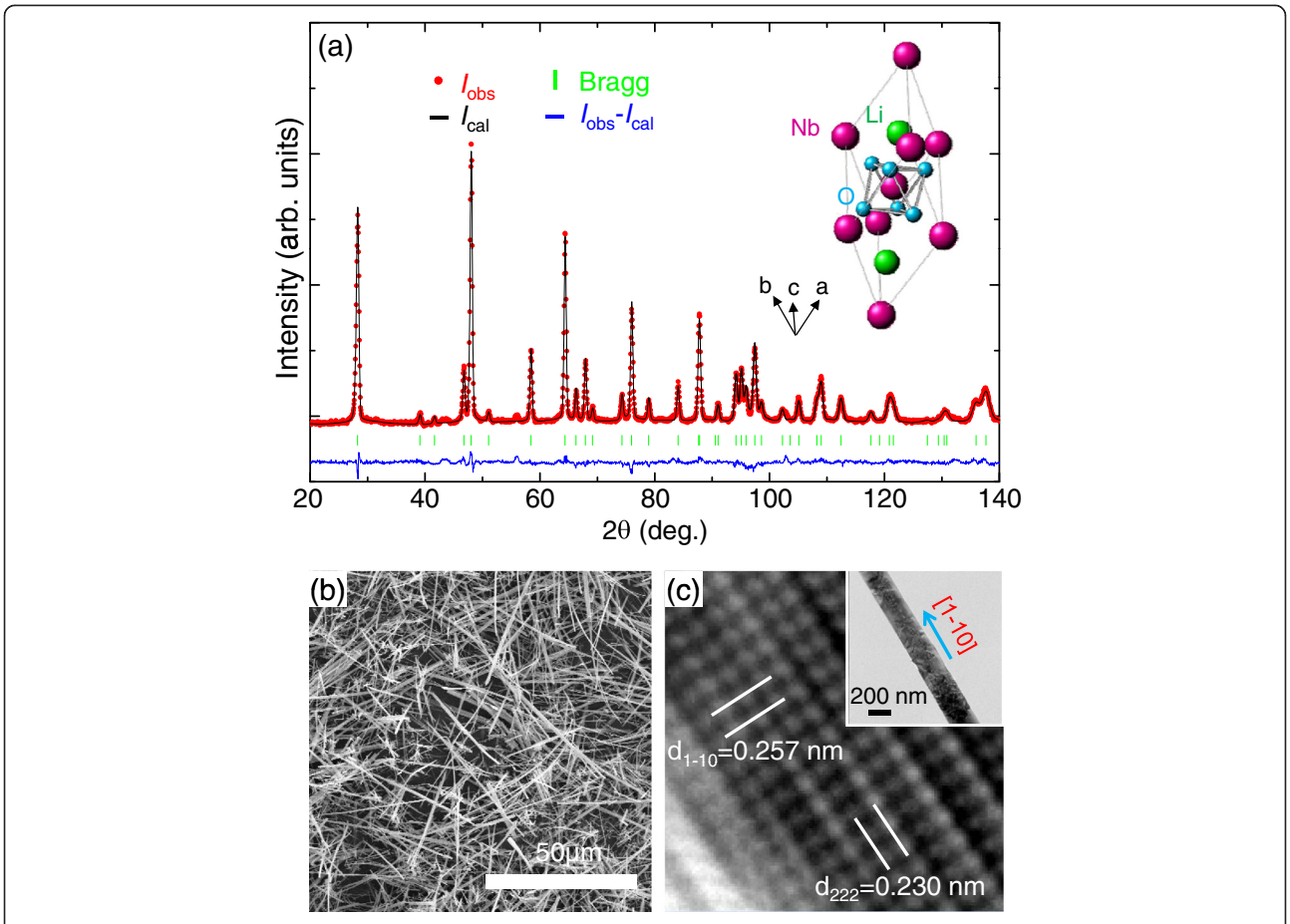

Figure 2 Structural characterization of $LiNbO_3$. (a) Rietveld analysis of neutron diffraction patterns of $LiNbO_3$. The red dots represent the observed intensity. The black lines represent the calculated intensity. The blue line corresponds to the difference between the observed and calculated intensities. The green line shows the Bragg reflection. In the inset of **(a)**, we show the crystal structure of $LiNbO_3$. **(b)** Field-emission scanning electron microscopy (FE-SEM) and **(c)** high-resolution transmission electron microscopy (HR-TEM) images of $LiNbO_3$. In the inset of **(c)**, we show a medium-resolution TEM image of a $LiNbO_3$ nanowire.

the linear portion of the piezoresponse amplitude signal as approximately 25 pmV^{-1}.

After confirming the piezoelectricity/ferroelectricity of the $LiNbO_3$ nanowire, we fabricated a composite nanogenerator for the e_{33} and e_{31} geometries, as schematically shown in Figure 4a,c, respectively. Even though the $LiNbO_3$ nanowires were randomly distributed inside the PDMS polymer, the piezoelectric/ferroelectric domains could be vertically aligned after applying a strong electric field for poling. If we were to apply stress, then the nanowires would be subjected to compressive strain, which would induce a piezoelectric potential due to the piezoelectricity of $LiNbO_3$. To screen the piezoelectric potential, positive and negative charges would accumulate at the top and bottom electrodes, respectively. Once the strain is released, the piezoelectric potential should diminish and the accumulated charges should move back in the opposite direction. Therefore, the continuous application and release of the strain will result in an alternating voltage and current [23].

To quantify the strain (ε), we used Young's modulus, Y, of the $LiNbO_3$-PDMS, Kapton, and PS films, having values of 0.87, 2.5, and 3.25 GPa, respectively [24]. The strain for the e_{33} geometry was then calculated using the equation $\varepsilon = P/Y$, where P represents the applied pressure. To quantify the strain for the e_{31} geometry, we calculated the strain neutral line from the equation $\Sigma Y_i t_i y_i = 0$ (for $i = 1$ to 4), where t and y represent the thickness of each layer and the distance from the strain neutral line to the center of each layer, respectively. The strain for the e_{31} geometry was obtained using the equation $\varepsilon = 2\,t' \times h/(a^2 + h^2)$, where a, h, and t' represent the half-width of the arc, the height of the arc, and the distance from the strain neutral line to the center of the $LiNbO_3$-PDMS composite layer, respectively [25].

Figure 4b,d shows the open-circuit voltage and closed-circuit current obtained for the e_{33} and e_{31} geometries, respectively. Through the polarity reversal test, we confirmed that the signals originated from the piezoelectricity of

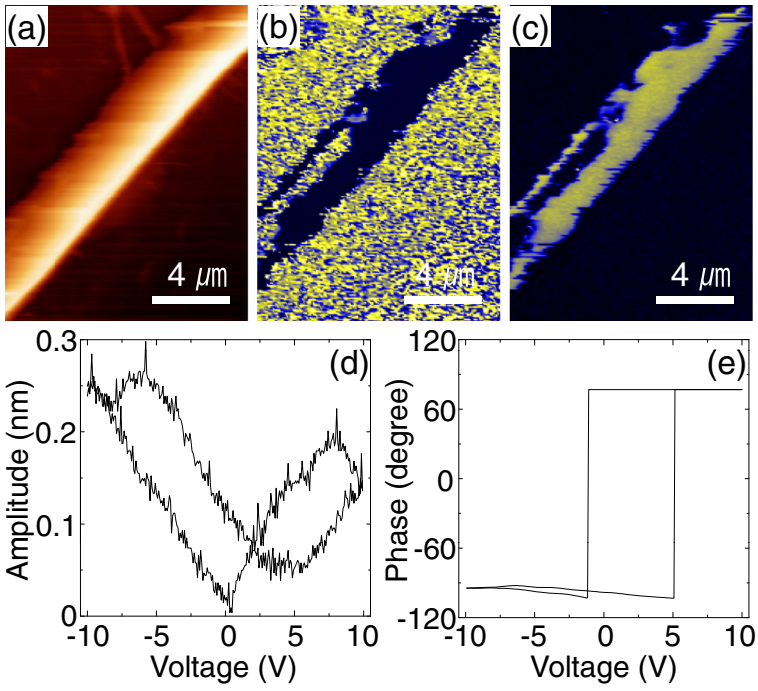

Figure 3 Piezoelectricity/ferroelectricity of the $LiNbO_3$ nanowire. (a) Topography, **(b)** piezoelectric amplitude, and **(c)** piezoelectric phase for a $LiNbO_3$ nanowire. Applied voltage dependences of **(d)** piezoelectric amplitude and **(e)** piezoelectric phase.

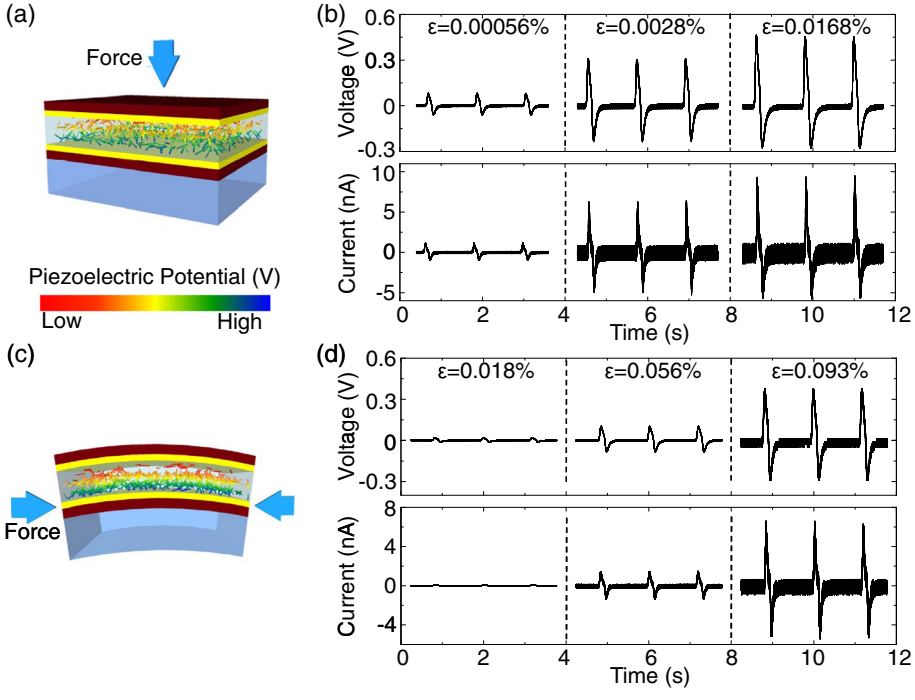

Figure 4 Schematic diagram and power generation for the $LiNbO_3$-PDMS composite nanogenerator. Schematic diagram of the $LiNbO_3$-PDMS composite nanogenerator for **(a)** e_{33} and **(c)** e_{31} geometries. Dark brown, yellow, and light blue represent the Kapton film, Au/Cr electrode, and PS film, respectively. The rainbow color of the $LiNbO_3$ nanowires represents the piezoelectric potential after the stress application. The open-circuit voltage (*V*) and closed-circuit current (*I*) at selected strains for **(b)** e_{33} and **(d)** e_{31} geometries.

$LiNbO_3$. With an increase in the strain, both the voltage and current increased as well. We note that the obtained voltage (current) for the e_{33} geometry was almost 20 times (100 times) larger than that for the e_{31} geometry for a similar value of the strain. For example, the open-circuit voltage and closed-circuit current (current density) for e_{33} with $\varepsilon = 0.0168\%$ were 0.46 V and 9.11 nA (4.64 $nA \cdot cm^{-2}$), respectively; whereas, for e_{31} with $\varepsilon = 0.018\%$, values of 0.02 V and 0.09 nA (0.044 $nA \cdot cm^{-2}$) were obtained, respectively. Note that due to the low output voltage and current for e_{31}, we could not detect a signal for strain lower than $\varepsilon = 0.018\%$. The electric power generated from the piezoelectric nanostructures was affected by the piezoelectric coefficient, dielectric constant, and strained length of the nanowire [9]. All of the other parameters were the same for both the e_{33} and e_{31} geometries, which implied that the significant difference in power generation was related to the different piezoelectric coefficients of $d_{33} = 27\ pmV^{-1}$ and $d_{31} = 4.3\ pmV^{-1}$ for $LiNbO_3$ [26].

The $LiNbO_3$-PDMS-based composite nanogenerator for the e_{33} geometry generates stable power even for excessive strain. In Figure 5a, we show the push-pull cycling number dependence of the open-circuit voltage and closed-circuit current. Over a period of 22 h, we continuously applied a compressive strain of up to 10^5 cycles. Within ±1%, the open-circuit voltage and closed-circuit current were quite stable. The stability of the dielectric constant and electric loss are shown in Figure 5b,c, respectively. The dielectric constant and current–voltage (*I-V*) characteristics were similar before and after the application of excessive strain (approximately 10^5 cycles).

In the $LiNbO_3$-PDMS composite nanogenerator, stable power generation depended on the mixing ratio. $LiNbO_3$ has high piezoelectricity, but is fragile and lossy. In contrast, PDMS has flexibility and a low dielectric constant, but no piezoelectricity. Nearly the same power generation, dielectric constant, and loss after excessive strain suggest that our $LiNbO_3$-PDMS composite nanogenerator was quite stable; this was attributed to the low volume ratio of $LiNbO_3$ inside the PDMS (approximately 1%). If the volume ratio of $LiNbO_3$ were to increase, then the power generation would increase as well at the expense of a larger dielectric constant; however, the composite devices may become fragile and lossy. Therefore, we suggest that optimization of the mixing ratio is crucial for the application of a lead-free piezoelectric composite nanogenerator.

Conclusions

We report a lead-free $LiNbO_3$ nanowire-based nanocomposite for piezoelectric power generation. Through the ion exchange of $Na_2Nb_2O_6$-H_2O, we synthesized long (approximately 50 μm) single-crystalline $LiNbO_3$ nanowires having a high piezoelectric coefficient (approximately 25 pmV^{-1}). By blending $LiNbO_3$ and PDMS polymer at a volume ratio

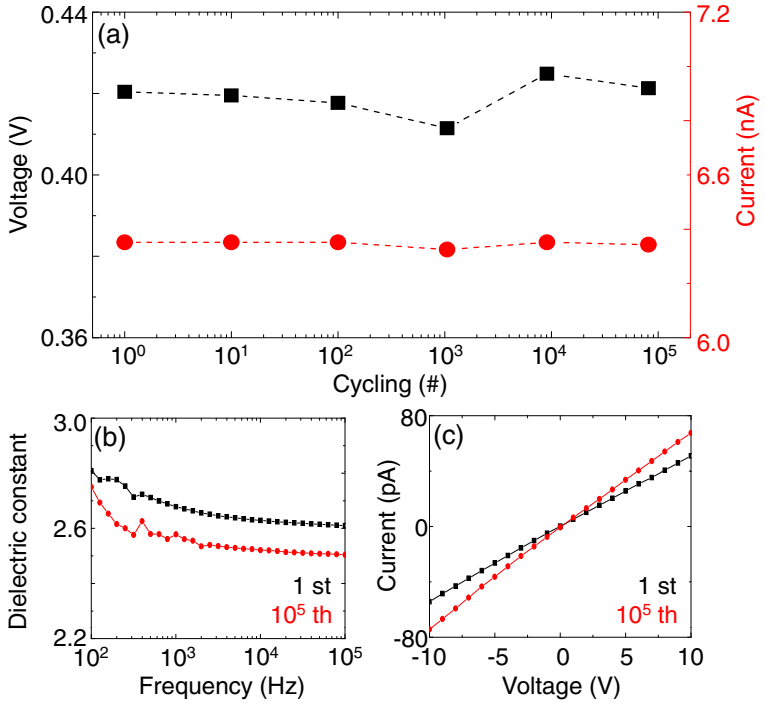

Figure 5 Stability of the $LiNbO_3$-PDMS composite nanogenerator. (a) Cycling number-dependent open-circuit voltage and closed-circuit current of the $LiNbO_3$-PDMS composite nanogenerator. **(b)** Dielectric constant and **(c)** current–voltage (*I-V*) characteristics before and after 10^5 cycles of excessive strain.

of 1:100, we fabricated a flexible nanocomposite nanogenerator. For a similar strain, the piezoelectric power generation for the e_{33} geometry was significantly larger than that for the e_{31} geometry due to the difference in the d_{33} and d_{31} piezoelectric coefficients of $LiNbO_3$. For up to 10^5 cycles of excessive strain, we observed that the output power, dielectric constant, and loss were quite stable. Optimization of the mixing ratio between lead-free piezoelectric materials and flexible polymers is an important factor to consider in the application of an energy-harvesting nanogenerator.

Competing interests
The authors declare that they have no competing interests.

Authors' contributions
BKY and YKP prepared the nanowire and performed the XRD, TG, DSC, SEM, and TEM measurements. BKY and ML fabricated the nanocomposite nanogenerator and tested the performance. NL and WJ carried out the PFM measurements and analysis. BKY and SL performed neutron diffraction measurements and the Rietveld analysis. JHJ designed the work and wrote the manuscript. All authors read and approved the final manuscript.

Acknowledgements
This work was supported by the National Research Foundation of Korea (NRF) grant funded by the Korean government (MEST) (No. 2012M2B2A4029408).

Author details
[1]Department of Physics, Inha University, Incheon 402-751, Republic of South Korea. [2]Department of Physics, Ewha Womans University, Seoul 120-750, Republic of South Korea. [3]Neutron Science Division HANARO, Korea Atomic Energy Research Institute, Daejeon 305-353, Republic of South Korea.

Received: 25 November 2013 Accepted: 19 December 2013
Published: 4 January 2014

References
1. Jaffe B, Cook WR, Jaffe H: *Piezoelectric Ceramics.* New York: Academic; 1971.
2. Saito Y, Takao H, Tani T, Nonoyama T, Takatori K, Homma T, Nagaya T, Nakamura M: **Lead-free piezoceramics.** *Nature* 2004, **432:**84–87.
3. Rödel J, Jo W, Seifert KTP, Anton E-M, Granzow T, Damjanovic D: **Perspective on the development of lead-free piezoceramics.** *J Am Ceram Soc* 2009, **92:**1153–1177.
4. Choi S-Y, Jeong S-J, Lee D-S, Kim M-S, Lee J-S, Cho JH, Kim BI, Ikuhara Y: **Gigantic electrostrain in duplex structured alkaline niobates.** *Chem Mater* 2012, **24:**3363–3369.
5. Wang ZL, Song JH: **Piezoelectric nanogenerators based on zinc oxide nanowire arrays.** *Science* 2006, **312:**242–246.
6. Park K-I, Xu S, Liu Y, Hwang GT, Kang SJL, Wang ZL, Lee KJ: **Piezoelectric $BaTiO_3$ thin film nanogenerator on plastic substrates.** *Nano Lett* 2010, **10:**4939–4943.
7. Wu JM, Xu C, Zhang Y, Yang Y, Zhou Y, Wang ZL: **Flexible and transparent nanogenerators based on a composite of lead-free $ZnSnO_3$ triangular-belts.** *Adv Mater* 2012, **24:**6094–6099.
8. Xu S, Hansen BJ, Wang ZL: **Piezoelectric-nanowire-enabled power source for driving wireless microelectronics.** *Nature Comms* 2010, **1:**93.
9. Xu S, Yeh Y-W, Poirier G, McAlpine MC, Register RA, Yao N: **Flexible piezoelectric PMN-PT nanowire-based nanocomposite and device.** *Nano Lett* 2013, **13:**2393–2398.
10. Jung JH, Lee M, Hong J-I, Ding Y, Chen C-Y, Chou L-J, Wang ZL: **Lead-free $NaNbO_3$ nanowires for a high output piezoelectric nanogenerator.** *ACS Nano* 2011, **5:**10041–10046.
11. Jung JH, Chen C-Y, Yun BK, Lee N, Zhou Y, Jo W, Chou L-J, Wang ZL: **Lead-free $KNbO_3$ ferroelectric nanorod based flexible nanogenerators and capacitors.** *Nanotechnology* 2012, **23:**375401.
12. Park K-I, Lee M, Liu Y, Moon S, Hwang G-T, Zhu G, Kim JE, Kim SO, Kim DK, Wang ZL, Lee KJ: **Flexible nanocomposite generator made of $BaTiO_3$ nanoparticles and graphitic carbons.** *Adv Mater* 2012, **24:**2999–3004.
13. Momeni K, Odegard GM, Yassar RS: **Nanocomposite electrical generator based on piezoelectric zinc oxide nanowires.** *J Appl Phys* 2010, **108:**114303.
14. Fluck D, Günter P: **Second-harmonic generation in potassium niobate waveguides.** *IEEE J Sel Topics Quantum Electron* 2000, **6:**122–131.
15. Zhao L, Steinhart M, Yosef M, Lee SK, Schlecht S: **Large-scale template-assisted growth of $LiNbO_3$ one-dimensional nanostructures for nano-sensors.** *Sens Actuators B* 2005, **109:**86–90.
16. Simoes AZ, Zaghete MA, Stojanovic BD, Gonzalez AH, Riccardi CS, Cantoni M, Varela JA: **Influence of oxygen atmosphere on crystallization and properties of $LiNbO_3$ thin films.** *J Eur Ceram Soc* 2004, **24:**1607–1613.
17. Zhu H, Zheng Z, Gao X, Huang Y, Yan Z, Zou J, Yin H, Zou Q, Kable SH, Zhao J, Xi Y, Martens WN, Frost RL: **Structural evolution in a hydrothermal reaction between Nb_2O_5 and NaOH solution: from Nb_2O_5 grains to microporous $Na_2Nb_2O_6 \cdot 2/3H_2O$ fibers and $NaNbO_3$ cubes.** *J Am Chem Soc* 2006, **128:**2373–2384.
18. Xu H, Nyman M, Nenoff TM, Navrotsky A: **Prototype Sandia octahedral molecular sieve (SOMS) $Na_2Nb_2O_6\ H_2O$: Synthesis, structure and thermodynamic stability.** *Chem Mater* 2004, **16:**2034–2040.
19. Goh GKL, Lange FF, Haile SM, Levi CG: **Hydrothermal synthesis of $KNbO_3$ and $NaNbO_3$ powders.** *J Mater Res* 2003, **18:**338–345.
20. Shinozaki Y, Mitsui T: **Powder neutron diffraction study of $LiNbO_3$.** *J Phys Chem Solids* 1963, **24:**1057–1061.
21. Santulli AC, Zhou H, Berweger S, Raschke MB, Sutter E, Wong SS: **Synthesis of single-crystalline one-dimensional $LiNbO_3$ nanowires.** *Cryst Eng Comm* 2010, **12:**2675–2678.
22. Jesse S, Baddorf AP, Kalinin SV: **Switching spectroscopy piezoresponse force microscopy of ferroelectric materials.** *Appl Phys Lett* 2006, **88:**062908.
23. Zhang Y, Liu Y, Wang ZL: **Fundamental theory of piezotronics.** *Adv Mater* 2011, **23:**3004–3013.
24. Zhou J, Gu YD, Fei P, Mai WJ, Gao YF, Yang RS, Bao G, Wang ZL: **Flexible piezotronic strain sensor.** *Nano Lett* 2008, **8:**3035–3040.
25. Lee M, Chen C-Y, Wang S, Cha SN, Park YJ, Kim JM, Chou L-J, Wang ZL: **A hybrid piezoelectric structure for wearable nanogenerators.** *Adv Mater* 2012, **24:**1759–1764.
26. Miller RC, Nordland WA, Bridenbaugh PM: **Dependence of second-harmonic-generation coefficients of $LiNbO_3$ on melt composition.** *J Appl Phys* 1971, **42:**4145–4147.

doi:10.1186/1556-276X-9-4
Cite this article as: Yun *et al.*: Lead-free $LiNbO_3$ nanowire-based nanocomposite for piezoelectric power generation. *Nanoscale Research Letters* 2014 **9**:4.